ELSEVIER

Chemical Geology 167 (2000) 129–140

CHEMICAL GEOLOGY
INCLUDING
ISOTOPE GEOSCIENCE

www.elsevier.com/locate/chemgeo

Hydrothermal formation of the calcium silicate hydrates, tobermorite ($Ca_5Si_6O_{16}(OH)_2 \cdot 4H_2O$) and xonotlite ($Ca_6Si_6O_{17}(OH)_2$): an in situ synchrotron study

S. Shaw [a,b,*], S.M. Clark [a,b], C.M.B. Henderson [a,b]

[a] *Earth Sciences Department, The University of Manchester, Manchester M13 9PL, UK*
[b] *Daresbury Laboratory, Daresbury, Warrington, Cheshire WA4 4AD, UK*

Received 11 January 1999

Abstract

In situ energy-dispersive X-ray diffraction (XRD) techniques have been employed to study the hydrothermal formation of crystalline tobermorite and xonotlite. Alkoxide gels of tobermorite composition with varying aluminium contents (Al/(Al + Si) = 0 to 0.15) were reacted with a saturated calcium hydroxide solution at temperatures varying from 190°C to 310°C on the saturated vapour pressure curve. Reaction products consisted of tobermorite, xonotlite or a mixture of both. Tobermorite is stabilised by increasing aluminium content and decreasing temperature, whereas xonotlite forms at higher temperature and lower aluminium contents. Reaction times ranged from 3 to 5 h, with the first Bragg peaks forming within the first 10 min. The formation mechanism involves a two-stage process. Firstly, a poorly crystalline C–S–H gel phase forms, which has good periodicity parallel to the *ab* plane but is poorly ordered parallel to the *c* direction. The second stage involves the ordering of the C–S–H gel along the (001) direction to form ordered crystalline tobermorite or xonotlite. Kinetic analysis indicates that the reaction rate is increased with increasing aluminium content and increasing temperature. Activation energies for these reactions at different aluminium contents were calculated from two datasets; firstly, from the change in 2θ position of the tobermorite(220)/xonotlite(320) peak during the reaction (19–30 kJ/mol) and secondly, from the rate at which the background hump intensity decreases for each experiment (26–33 kJ/mol). © 2000 Elsevier Science B.V. All rights reserved.

Keywords: Calcium silicate hydrates; Tobermorite; Xonotlite

1. Introduction

The calcium silicate hydrate (C–S–H) minerals, tobermorite ($Ca_5Si_6O_{16}(OH)_2 \cdot 4H_2O$) and xonotlite ($Ca_6Si_6O_{17}(OH)_2$), are rare minerals formed in hyper-alkaline, hydrothermal environments. They usually occur where hydrothermal fluids react with basic igneous rocks, e.g., Okayama, Japan (Henmi and Kusachi, 1992) and Skye, UK (Livingston, 1988). These phases and their gel precursors are also known to form in cements and in the hyper-alkaline environments surrounding cementitious nuclear and toxic waste sites (Atkinson et al., 1995). Consequently, an

* Corresponding author. Earth Sciences Department, The University of Manchester, Williamson Building, Oxford Road, Manchester M13 9PL, UK. Tel.: +44-958-917783.
E-mail address: shaw@fs1.ge.man.ac.uk (S. Shaw).

0009-2541/00/$ - see front matter © 2000 Elsevier Science B.V. All rights reserved.
PII: S0009-2541(99)00205-3

increased understanding of the processes that form these minerals will help to determine the chemical evolution of the cement–rock interface of these sites related to porosity, permeability and ground water chemistry changes over a geological time scale.

The C–S–H system is highly complex with over 30 stable phases reported and the relative stabilities of some of these phases are shown in Fig. 1. This complexity is increased by the existence of many poorly ordered gel (e.g., C–S–H gel) and metastable crystalline phases (e.g., *Z*-phase). These compounds make experimental work in this system very complicated with single-phase, pure, highly crystalline material difficult to synthesise. The mineral, tobermorite, is stable over a range of compositions from Ca/Si = 0.8 to Ca/Si = 1. This variation is possibly due to the nature of the tobermorite structure and the intrinsic disorder within it (Hamid, 1981). Xonotlite forms at higher temperatures than tobermorite, with the equilibrium phase boundary between the two minerals being at approximately 140°C (Gabrovšek et al., 1993), although tobermorite can be produced metastably at temperatures well above 200°C. The phase defined as C–S–H gel is highly disordered. A great deal of work has been carried out on this phase as it is one of the primary components of Portland cement (Taylor, 1990). Despite this work, the thermodynamic, chemical and structural properties of CSH(I) are poorly understood (Gartner and Jennings, 1987).

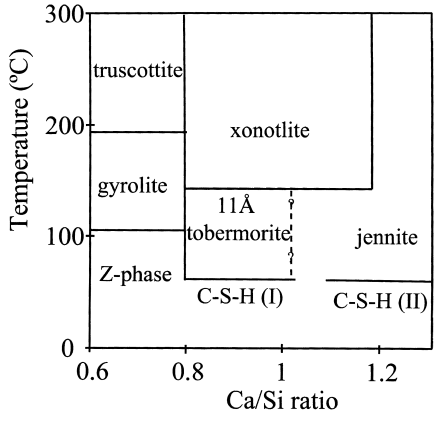

Fig. 1. Schematic stability diagram showing the existence of hydrated calcium silicates under hydrothermal conditions.

The 11 Å-tobermorite structure is normally orthorhombic, although recently a monoclinic form has been described by Hoffman and Armbruster (1997). Three polytypes of tobermorite exist, namely 14, 11 and 9 Å tobermorites, with their names relating to the *d*-spacings of the (002) Bragg peaks. The variation in the length of the *c*-axis depends on the amount of water in the tobermorite structure, respectively, 8, 4 and OH_2O molecules per formula unit. The structure of 11 Å tobermorite consists of a central layer of calcium octahedra which has silicate sheets on each side (Hamid, 1981). The silicate sheets consist of infinite silicate chains parallel to *b*, with a three-tetrahedron, 'dreierketten' repeat, similar to chains in wollastonite. This particular three-tetrahedron repeat, as opposed to a pyroxene-type chain, reflects the way in which the silicate tetrahedra are bonded to the calcium layer. The calcium octahedra share oxygens with the silicate tetrahedra, and the distance between two edges in the calcium octahedral layer is about the same length as a three-silicate tetrahedra repeat unit. The composite layers of one calcium and two silicate layers are bound together by an interlayer containing calcium ions and water molecules (see Fig. 2a). The interlayer contains variable amounts of calcium, with the resulting charge alteration caused by this variation in occupancy being compensated for by a variation in the number of hydrogen atoms bonded to the silicate chains. Therefore, the variable occupancy of calcium in these layers allows the Ca/Si ratio in tobermorite to vary (Hamid, 1981).

The 11 Å tobermorite is the most common form found in nature and can be described as 'normal' or 'anomalous' depending on its dehydration behaviour. Normal tobermorite dehydrates to the 9 Å form at approximately 300°C. However, although the anomalous form dehydrates under similar conditions, its *c*-axis does not decrease significantly. The structural interpretation for this phenomenon is thought to be due to the existence of cross-linkages of silicate layers across the interlayer in anomalous tobermorite (Mitsuda and Taylor, 1978), which prevents a reduction in the interlayer space when water molecules are lost.

Xonotlite is structurally very similar to tobermorite but has double chains running parallel to the *b*-axis which form layers in the *ab* plane (Mamedov

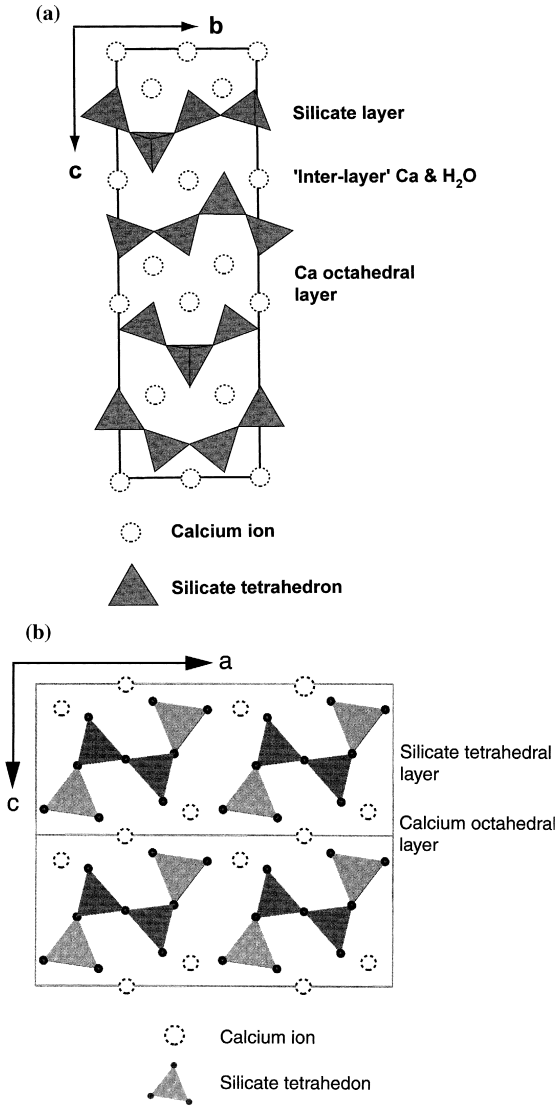

Fig. 2. (a) A *bc* projection of the structure of tobermorite. Note the three tetrahedron repeat (dreierketten) in the silicate chains parallel to *b*. (b) An *ac* projection of the structure of xonotlite. The silicate layers contain double chains of silicate tetrahedra aligned parallel to *b*.

and Belov, 1955) rather than the single chains found in tobermorite. The structure consists of alternating layers of calcium polyhedra and of silicate layers perpendicular to the *c*-axis (Fig. 2b). The structure of C–S–H gel is more disordered than those of crystallines, tobermorite and xonotlite, and has been the subject of much debate in recent years. There are several different models for the structure of this phase including the 'defect tobermorite' model (Cong and Kirkpatrick, 1996; Klur et al. 1998). This model bases the structure of C–S–H gel on that of tobermorite, with significant concentrations of a number of different types of defects, the most important of these being that the silicate chains have missing tetrahedra and chain segments.

There has been a lot of work in this field aimed at understanding the structural relations, formation mechanisms and growth kinetics of the C–S–H phases. Mitsuda and Taylor (1975) and Gabrovšek et al. (1993) studied the influence of aluminium on the formation of tobermorite under hydrothermal conditions. Compositions with Al:Si ratios ranging from $Al/(Si + Al) = 0$ to $Al/(Si + Al) = 0.15$ were studied; increasing the aluminium content beyond this level causes the precipitation of hydrogarnet as a secondary phase. The crystallization rate was found to increase with increasing aluminium content and temperature, but no quantitative kinetics was calculated. Further work by El-Hemaly et al. (1977) showed that metastable tobermorite can be produced, existing for up to 48 h at 180°C before transforming to xonotlite. The phase boundary between these two phases is approximately 140°C, but equilibration at this temperature takes up to 2 months (El-Hemaly et al., 1977). Thus, it appears that the reaction mechanisms and kinetics of this system are slow and highly complex. A formation mechanism for tobermorite was proposed by Jauberthie et al. (1996) from X-ray diffraction (XRD) analysis of hydrothermally synthesised tobermorite samples at various stages of crystallization. They suggest that, initially, sheets roughly parallel to the *ab* plane form, which then order along the *c*-axis. None of the previous synthesis studies has reported the formation of the monoclinic form of tobermorite. This could be due to unusual formation conditions in nature, which have not yet been reproduced in the laboratory. However, a more likely explanation is that the poor crystallinity of the reaction products, combined with the similarity of the orthorhombic and monoclinic structures, makes the two symmetries difficult to distinguish with powder diffraction methods. Despite all these previous works, little quantitative information has been obtained, mainly because in all of these studies the reaction

had to be quenched before any sample characterisation could be performed.

The present study was initiated to investigate, in situ, the hydrothermal formation of tobermorite and the higher temperature phase, xonotlite. The main aims were to investigate quantitatively the influence of temperature and aluminium content on phase stability, reaction kinetics and reaction mechanisms.

2. Methods

Energy-dispersive powder diffraction (EDPD) was the technique of choice for this study. This method involves shining a beam of polychromatic X-rays upon a sample and using an energy-sensitive solid state detector, set at a fixed diffraction angle (2θ), to record the diffraction pattern as a function of energy. This method has the advantage that the whole powder diffraction pattern is collected simultaneously, allowing rapid time-resolved measurements. Also, the post-sample collimation excludes any contribution from the surrounding sample environment to the collected diffraction patterns, giving patterns free from any ambiguous unindexed peaks. A synchrotron source of X-rays is necessary for this energy-dispersive work since it gives a continuous smooth spectrum of X-rays up to very high energies (range typically 5–120 keV).

The in situ synthesis experiments for this work were performed on station 16.4 (Clark, 1996) at the Synchrotron Radiation Source (SRS), Daresbury Laboratory, UK and on station 13-BM-D at the Advanced Photon Source (APS), Argonne National Laboratory, USA. Both these stations have a white beam X-ray source, supplied by a bending magnet on 13-BM-D and a 6-T wiggler on station 16.4.

The arrangement for both sets of experiments was basically the same (Fig. 3). A set of pre-sample slits was used to reduce the incident beam flux to a level consistent with the maximum count rate of the detector systems (3×10^4 counts/s). On 13-BM-D, this consisted of two sets of tungsten carbide cubes, which limited the beam in the horizontal and vertical direction. A beam size of 200×50 μm^2 was ideal for the experiments being performed. On 16.4, the pre-sample beam reduction consisted of a pin-hole (Evans et al. 1994; Clark et al., 1995). Once the incoming beam has passed through the slits, it is transmitted through windows in the cell heater unit and the reaction vessel walls.

The reaction cell is a modified rod bomb (Anton Parr; Part number 4711) with a section of the wall milled down to the required wall thickness (Fig. 4) to allow sufficient X-ray transmission (Clark et al. 1995). The greater the wall thickness, the greater the reduction in X-ray transmission, but the higher the reaction temperature possible. The cell is open to a head unit at the top, which has a pressure transducer and a pressure safety valve. The bomb contains either a PTFE or copper liner depending on the operating temperature; at greater than 315°C, copper

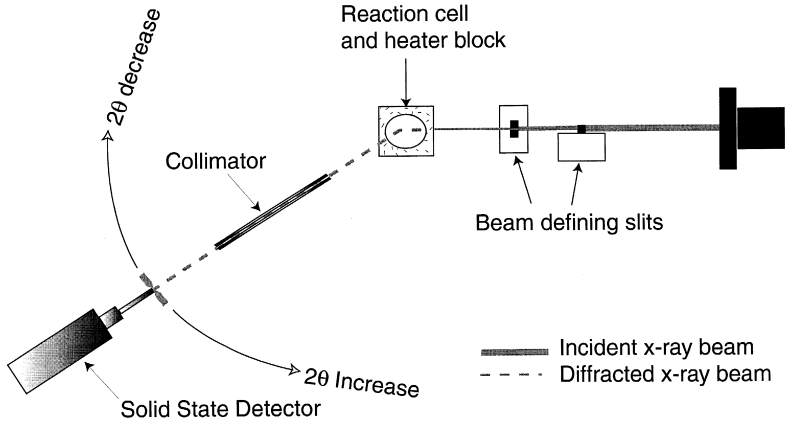

Fig. 3. Schematic diagram showing the on-line, in situ, hydrothermal experimental set-up on Station 13-BM-D of the APS.

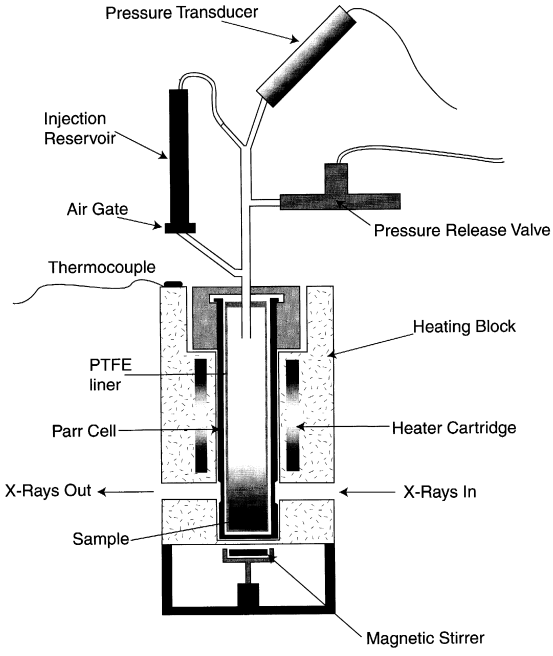

Fig. 4. Schematic diagram of a vertical section through the on-line hydrothermal reaction cell and heater unit.

was required as PTFE breaks down at this temperature. Heating is achieved by placing the Parr cell in an aluminium block, which is heated by four resistance cartridge heaters. The heater block unit has incident and exit slits for the incoming and outgoing X-ray beam located in line with the milled-down area of the Parr cell. This allows the X-rays to pass through as small a thickness of steel as possible. The temperature is maintained remotely using a constant current on/off controller with a K-type control thermocouple attached to the top of the block (Fig. 4). For the three lowest temperature runs, this system was not available and the temperature was controlled using a variable resistor. This produced an increased error on the reaction temperatures for these experiments.

The maximum temperature currently achievable in these experiments at the SRS is limited to about 240°C by the wall thickness of the bomb, which at 0.4 mm is the thickest that the X-rays produced by the 6-T wiggler insertion device on line 16 of the SRS can penetrate and give usable diffraction data on the required time scale. The APS is a third-generation synchrotron source, which is a significant improvement on the SRS for these types of experiment. The X-ray energy/flux profile of a bending-magnet beamline has at least 10 times the flux of a beam line at the Daresbury source and achieves high brightness up to 130 keV. This increased energy range gives improved penetrating power to the X-ray beam, allowing it to pass through a reaction cell with walls up to 3 mm thick. Thus, hydrothermal experiments at the APS can be carried out at increased temperatures, up to about 330°C.

The X-ray beam is diffracted by the cell contents, the cell itself, and the heater unit to various angles of 2θ depending on the energy of the particular X-ray photons within the beam and the *d*-spacing of the crystalline material. A post-sample collimator consisting of 300-mm long slits spaced 0.1 mm apart was placed at a particular angle of 2θ in order to give the desired range of *d*-spacing. This tight post-sample collimation ensures that only diffraction from the material inside the cell is detected excluding all diffractions from the cell and heater unit. On 16.4, three molybdenum collimators were used, each positioned at a slightly different angle to each other. Placed at the end of these slits were three Canberra energy-dispersive detectors. This setup allows a large range of *d*-spacings to be observed; typically a range from 20 to 1.5 Å was chosen. On 13-BM-D, one brass collimator was used with one energy-dispersive Canberra detector positioned at the end. This system limits the observable *d*-spacing range significantly; typically a range from 4.5 to 2.5 Å was chosen.

The starting material for the reactions consisted of a calcsilicate alkoxide gel (Hamilton and Henderson, 1968) with the stoichiometric composition of natural tobermorite ($Ca/(Si + Al) = 0.83$). The gels were fired at 500°C, which is considerably lower than the 800°C quoted by Hamilton and Henderson (1968). This lower temperature was chosen to avoid crystallisation of the anhydrous gel, but is not high enough to remove all the water present. Typical weight yields for the gels were relatively high, ranging from 99.5% to 101.5%. Although every effort was made to produce a completely amorphous gel, XRD analysis of some batches showed one or two small diffuse Bragg peaks, which could be tentatively assigned to some crystalline Ca_2SiO_4 polymorphs. When present, this impurity proved to be insignificant as it made up only a small percentage

of the starting gel and became undetectable within the first 5 min of each experimental run.

The aluminium content of the starting materials varied from 0% to 15% of aluminium substituted for silicon. Saturated calcium hydroxide aqueous solution was added to the solid in the ratio of 5:1 by weight. This solution was chosen because it is approximately the composition of the highly alkaline (pH = 12) ground water that is expected to form around a cementitious waste site (Atkinson et al., 1995). Once sealed, the cell was placed inside the heating block at the required temperature. Reactions were performed at temperatures varying from 235°C to 310°C with all the experiments above 240°C carried out at the APS. As the mixture was heated, the gel begins to react and crystalline phases form. The sample was constantly X-rayed during the reaction with a single pattern being taken every 1 or 2 minutes depending on the reaction rate.

3. Results and data analysis

All the experiments were completed within 5 h, with the main period of growth always being within the first 60 min. Crystalline tobermorite, xonotlite or a mixture of both was produced as the endproduct, depending on the reaction temperature and the starting composition. Fig. 5 shows a time-resolved XRD pattern from one of the in situ hydrothermal experiments. Initially, the XRD pattern contains a large background hump with no significant Bragg peaks. This hump is due to scattering from the amorphous starting material and the calcium hydroxide solution present within the reaction cell. Within the first few minutes (< 5 min), Bragg peaks begin to appear as the amorphous gel begins to crystallize. The different Bragg peaks of the crystallising phase(s) do not all appear simultaneously but emerge in a distinct sequence defined by the reaction mechanism. The growth of the Bragg peaks coincides with a decrease in the area of the background hump as the amount of amorphous material present decreases. After a period of rapid peak growth, there is no real change in the patterns, apart from some peak narrowing as the crystalline phase becomes more ordered. In this case, the final product was tobermorite with no xonotlite present.

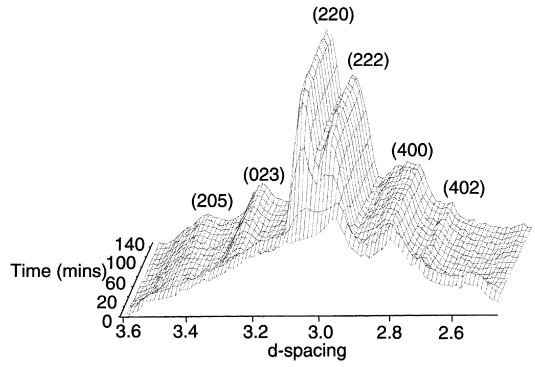

Fig. 5. Time-resolved EDPD pattern showing the formation of tobermorite from an amorphous gel as a function of time. Reaction performed at 250°C with starting composition of 15% aluminium replacing silicon. Bragg peaks index using JPCDS card 45-1480.

The Bragg peaks for tobermorite and xonotlite were indexed using the JPCDS cards, 45-1480 and 29-0379, respectively. Tobermorite was assumed to be orthorhombic because the poor crystallinity of the reaction products and the relatively low resolution of the EDPD technique make it impossible to distinguish between the orthorhombic and monoclinic types of tobermorite. When a mixture of xonotlite and tobermorite is produced, it can be difficult to differentiate between the two as they have very similar XRD traces in the region observed. The main differences between their two XRD patterns are a peak at 2.98 Å (222), which is unique to tobermorite, and one at 4.21 Å (400), which is only due to xonotlite. In the runs which produced a mixed phase endproduct, tobermorite seems to be the first phase to crystallize. As the reaction proceeds, the main tobermorite defining peak at 2.98 Å (222) decreases while all the other peaks, which are present in xonotlite, continue to grow. Although the reactions were stopped after a few hours, the tobermorite peak was still decreasing in intensity, indicating that, with time, pure xonotlite would be produced as the final stable phase.

Table 1 shows the cell parameters for final reaction products calculated from the EDPD data obtained when the sample was at temperature under hydrothermal conditions. The first dataset comes from an experiment that produced pure tobermorite (Al/(Al + Si) = 0.15) and the second from a run

Table 1
Cell parameters calculated from two synthetic reaction products compared with published data for the two mineral phases

Cell parameter (Å)	Tobermorite		Xonotlite	
	Synthetic (Al 15%) 240°C	Natural sample (JCPDS 45-1480)	Synthetic (Al 0%) 270°C	Natural sample (JCPDS 29-0379)
a	11.37 ± 0.06	811.233	17.19 ± 0.03	17.029
b	7.34 ± 0.05	7.372	7.44 ± 0.01	7.356
c	22.6 ± 0.4	22.56	7.121 ± 0.009	7.007
β	–	–	89.9 ± 0.1	90.34

which produced pure xonotlite (Al/(Al + Si) = 0). The unit cell parameters for tobermorite were calculated assuming an orthorhombic unit cell and six peaks were used for both unit cell refinements. The cell parameters were refined using the program, Unit Cell (Holland and Redfern, 1997), and show good agreement with the published room temperature data for these mineral phases. The slightly higher values calculated from the experimental data are probably due to the elevated temperature.

To analyse the kinetics of these reactions, every diffraction pattern in each isothermal experiment was peak-fitted using the PC-based program, Xfit (Cheary and Coelho, 1992). The Bragg peaks were fitted with pseudo-Voigt peaks and the background hump fitted with a split Pearson peak. The changes in the peak area, 2θ position, and the full width at half maximum (FWHM) of the peak with time can be used to determine the reaction kinetics and help devise a reaction mechanism. The kinetics model chosen is an Avrami-type equation of the form given below:

$$\alpha = 1 - e^{-(k(t-t_0))^n},$$

where α is the fraction completed, k is the rate constant for the reaction, t is the time, t_0 is the time the reaction began, and n is a constant that depends on the reaction mechanism.

Initially, all the datasets were fitted with n as a variable parameter. However, it was soon found that values for n calculated this way were highly variable (about 0.8–2.3) and showed no trends with composition and/or temperature. Such variations in n are unlikely to be real as they would indicate different reaction mechanisms for closely similar starting materials under similar reaction conditions. Therefore, values of $n = 1$ and $n = 2$ were chosen and all the kinetics datasets were fitted with these two values. Over 80% of the datasets fitted better with $n = 1$ than $n = 2$, with no trend with temperature or composition. Thus, for internal consistency, we have chosen to fit all the datasets with $n = 1$, but note that we do not attempt to use the n value in interpreting the reaction mechanism.

Errors in the peak fitting parameters, e.g., 2θ position and peak area, calculated from Xfit, were propagated through all the kinetics analysis to the activation energy determinations.

4. Discussion

The sequence in which the Bragg peaks form during the crystallization reactions shows a clear pattern, even for experiments that produced different endproducts. The first peaks to form are at ≈ 3.0 Å, which is in the same position as the tobermorite (220) and (222) peaks and the xonotlite (320) peak. At the same time, a peak at ≈ 1.8 Å forms, which is in the position of the tobermorite (040) and xonotlite (040) peaks. These peaks indicate the presence of C–S–H gel and can be correlated with particular features within the C–S–H structure. Vieland et al. (1996) correlated the peak at 3.0 Å with the Ca–Ca physical repeat distance within the structure (Fig. 6), and the 1.8 Å peak with the presence of dreierketten chains. At this stage, the material has the proposed 'defect tobermorite' structure (Cong and Kirkpatrick, 1996) with disordered silicate chains and CaO layers with relative good periodicity parallel to the *ab* plane, but there is no long-range periodicity along the *c*-axis. The indices of most of the Bragg peaks observed reinforce this model as they have little or no component in the (00*l*) direction. The only excep-

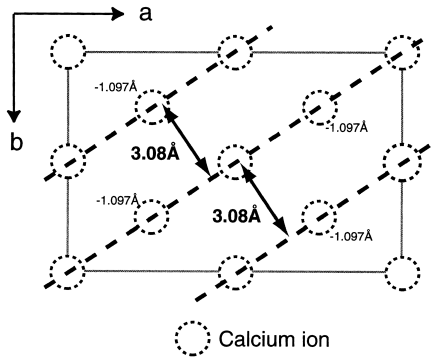

Fig. 6. An *ab* projection of calcium ions in the octahedral layer of tobermorite. The spacing between these rows of calcium ions in this plane is 3.08 Å.

tion to this is the tobermorite (222). The reason why this peak appears and the tobermorite (002) does not, e.g., is due to the difference in the *d*-spacings of the two Bragg peaks and their orientation within the tobermorite structure. The tobermorite (222) has a *d*-spacing of 2.98 Å and (002) a *d*-spacing of 11.3 Å. For a Bragg reflection to be observed, about 5–10 ordered lattice repeats perpendicular to the diffracting crystallographic plane are required. In the case of the tobermorite (222) peak, 5–10 repeats along the (222) direction would require that there be crystalline regions, which have good atomic ordering parallel to the *c*-axis of at least 6–10 Å. This indicates that, if there is reasonably good order in the *ab* plane, it would require only a small degree of order parallel to the *c*-axis to get intensity in the (222) peak. In contrast, for the (002) peak to be present, it would require significantly more order parallel to the *c* -axis of at least 60–100 Å.

Shortly after this stage of the reaction, the tobermorite (400) ($d = 2.8$ Å) peak and/or the xonotlite (-321) and (402) peaks form. The other Bragg peaks for these phases form shortly afterwards, including the basal peaks, i.e., tobermorite (002) and xonotlite (001). These were only observed in the three experiments performed on station 16.4, which has a three-element energy-dispersive detector allowing a large *d*-spacing range to be monitored. The other experimental runs were performed using a single-element detector that did not collect data in the *d*-spacing range in which the basal peaks appear. This overall sequence indicates that after the formation of the C–S–H gel structure, the CaO layers and silicate chains became more ordered with increasing periodicity in the (001) direction to form the complete tobermorite or xonotlite structure.

From the results of these experiments, a clear pattern of phase stability can be seen when the temperature, composition and reaction products are examined together (Fig. 7). In summary, it seems that as the aluminium content is increased and temperature decreased, tobermorite becomes the more stable phase, and conversely, as temperature is increased and aluminium content decreased, xonotlite becomes the more stable phase. The area marked as a mixed zone is unlikely to be thermodynamically stable but is probably a product of slow reaction kinetics. Previous studies (El-Hemaly et al., 1977) in this system show that the phase boundary between tobermorite and xonotlite occurs at a much lower temperature, approximately 140°C. However, in the same studies, it was also found that tobermorite can be produced metastably at temperatures above 140°C. Therefore, the phase existence fields shown in Fig. 7 represent the phase stability on the time scale of this group of experiments (3–5 h).

Kinetic information from the changes in integrated intensity and FWHM of the Bragg peaks as they grew proved difficult to obtain. There are several possible reasons for this. Firstly, many of the reactions produced a mixture of tobermorite and xonotlite, and because these two phases have very similar diffraction patterns, they have many overlap-

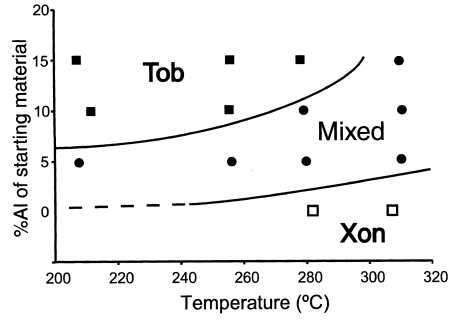

Fig. 7. Final reaction products plotted against temperature and aluminium content. The phase existence fields given represent the stability over a 3–5 h time period.

ping peaks. Therefore, virtually all the peaks are a binary mixture of at least one tobermorite peak and one xonotlite peak. During the experiments, the relative amount of each of these phases varies, depending on whether a given phase continues to form, transform or perhaps resorb. Therefore, it is extremely difficult to quantify how much of each component is present at any one time. Secondly, the first few percentages of crystalline product are not observed by diffraction. This makes a reaction rate model difficult to fit as the first part of the reaction is very important kinetically. Although the kinetics cannot be fully resolved, the formation of each peak shows a clear two-stage growth process, which initially involves peak formation and area increase, followed by a reduction in the peak width and a slight shift in 2θ position. The peak-growth stage indicates the formation of crystalline material and the peak-narrowing stage indicates an increase in order in this crystalline phase. The shift in 2θ position is probably also indicative of ordering in the structure. These results reinforce the evidence that initial formation of a poorly ordered gel is progressively followed by an ordering mechanism for the formation of tobermorite and xonotlite in this system.

The most reliable kinetic data based on the Bragg peaks were obtained from the change in 2θ position of the tobermorite (220) and/or the xonotlite (320). Also, these peaks are very well-defined and are not overlapped by any other peaks. Fig. 8a shows data for the change in 2θ position, scaled from 0 to 1,

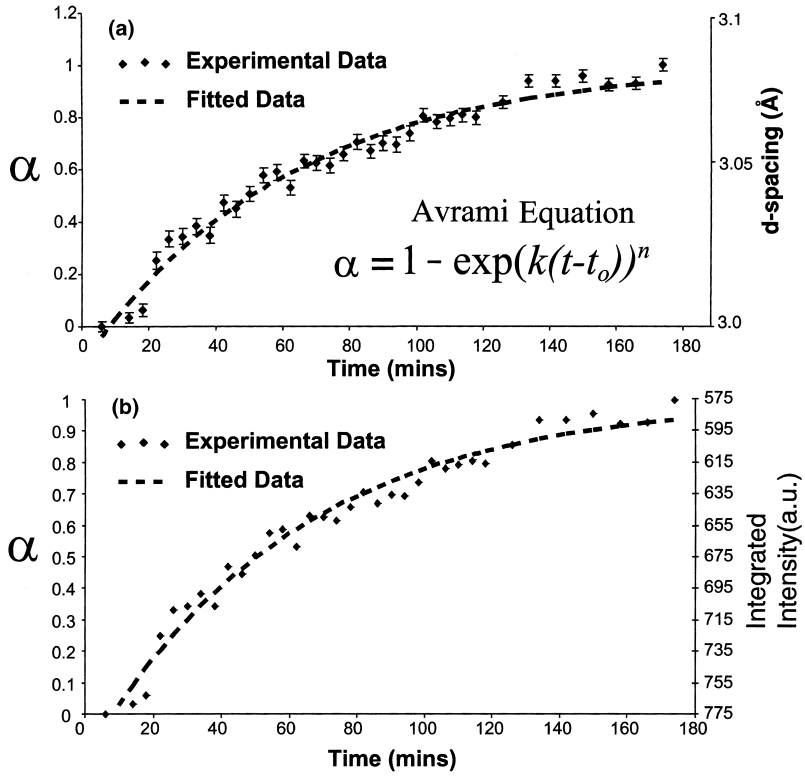

Fig. 8. (a) Experimental data from the change in 2θ position of the tobermorite (220) and/or the xonotlite (320) peak scaled from $\alpha = 0$ to 1 and plotted against time in minutes; the right-hand vertical scale shows the *d*-spacing shift with time. Data are from a reaction performed at 205°C with a starting material composition of Al/(Al + Si) = 0.10. (b) Experimental data from the change in the background hump intensity scaled from 0 to 1 and plotted against time in minutes; the right-hand axis shows the integrated intensity change with time. Data are from a reaction performed at 205°C with a starting material composition of Al/(Al + Si) = 0.5. Data are fitted with an Avrami kinetics model where α is the degree of reaction and k is the rate constant.

and plotted against time for one experimental run. An Avrami-type model is fitted to the data using a least squares fit with n fixed at 1 and k and t_0 allowed to vary. Values for t_0 varied from 14 to 35 min. The change in position of this peak was from about 3.0 Å when first formed, to 3.09 Å in the crystalline phase. This peak shift probably relates to ordering within the calcium octahedral layers, perhaps influenced by ordering in the silicate layers. The latter process is likely to involve an increase in the dreierketten chain lengths due to the inclusion of tetrahedra into vacancies in the chains. Therefore, due to the nature in which the silicate chains are bonded to the calcium layers, the now rigid, continuous silicate chains define the distance between the planes of calcium ions (3.09 Å).

If the k values of the 2θ position shift for each experiment are plotted against temperature, a clear trend can be seen (Fig. 9). As temperature is increased, k increases and as the aluminium content increases, k also increases, indicating that increasing the aluminium content increases the reaction kinetics.

Fitting data for the decrease in the background hump area can also be used to determine the kinetics in this system. This is because the background area is inversely proportional to the amount of crystalline material formed and is not phase-dependent. Each dataset was fitted with an Avrami-type kinetics model as described above (e.g., Fig. 8b). The t_0 values for these experiments vary from 5 to 20 min within which time there is usually a slight increase in the background area ($\approx 5\%$). This increase is probably due to the hydration and breakdown of the small amount of crystalline Ca_2SiO_4 present in the starting material. When the k values from each experiment are compared, a pattern very similar to that obtained from the previous dataset can be seen (Fig. 10). As the temperature increases, the reaction rates increase and as the aluminium content increases up to 10%, the reaction rate increases. The reaction rates of the 15% aluminium runs are lower than those for the 10% aluminium runs, indicating that the maximum rate would occur for compositions with between 5% and 15% aluminium.

Activation energies for each of the three aluminium contents in each of the two datasets can be calculated from an Arrhenius plot (Fig. 11). Table 2 contains the calculated activation energies for both datasets for each starting material composition. The activation energies obtained from the change in 2θ

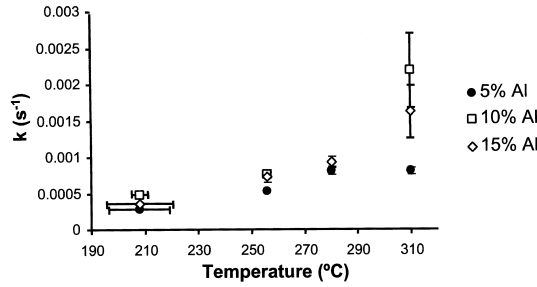

Fig. 10. Rate constant (k) values calculated from the decrease in background area for each experimental run plotted against temperature.

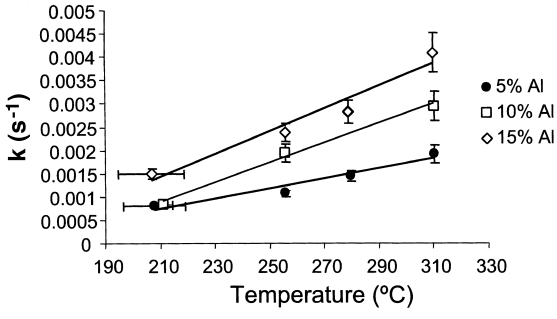

Fig. 9. Rate constant (k) values calculated from the change in 2θ position of tobermorite (220) and/or xonotlite (320) peak for each experimental run plotted against temperature.

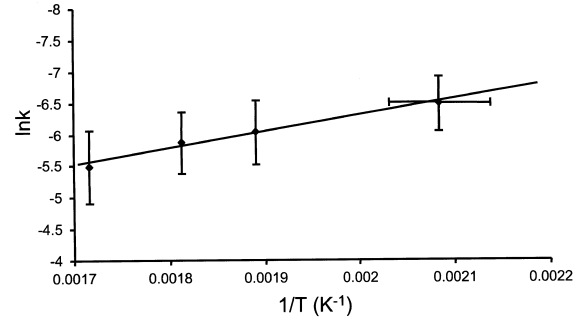

Fig. 11. Arrhenius plot of data from the change in 2θ position of the tobermorite (220) and/or xonotlite (320) peak. Data shown for experimental runs with 15% aluminium replacing silicon.

Table 2
Activation energies calculated form both the decrease in background area and the change in the 2θ position of the tobermorite (220) and/or xonotlite (320) peak

Composition of starting material (% Al)	2θ position of tobermorite (220) and/or xonotlite (320) (kJ/mol)	Background area (kJ/mol)
5	19 ± 3	26 ± 5
10	30 ± 6	37 ± 18
15	22 ± 2	33 ± 3

position of the tobermorite (220) and/or the xonotlite (320) peak are quite similar despite the large error on the activation energy for the 10% aluminium content. The activation energies calculated from the background area data are also reasonably consistent but are somewhat higher than the values from the previous dataset. The reason for this is not clear, but one possible explanation is that the change in 2θ position of the tobermorite (220) and/or the xonotlite (320) peak and the change in background area represent different stages in the crystallization process. The reduction in background area is not phase-dependent and will decline as the crystalline phase is forming and/or ordering, and therefore represents the entire reaction from amorphous starting material to ordered crystalline phase. In contrast, indicating that the change in 2θ position may characterise the ordering phase of the reaction only. Therefore, the difference in activation energy reflects the different stages of the crystallisation process that the two datasets represent.

5. Conclusions and wider implications

(1) Results from this study indicate that, on the time scale of the experiments performed (3–5 h), tobermorite is stabilised by increasing aluminium content of the starting material and by decreasing temperature, whereas xonotlite is stabilised by decreasing aluminium and increasing temperature.

(2) The formation mechanism for both tobermorite and xonotlite involves a two-stage crystal growth then ordering process. Firstly, crystalline domains with good periodicity parallel to the *ab* plane, but little order in the (001) direction, form, making material very similar to C–S–H gel. Following this stage, the gel orders parallel to the *c*-direction, thus producing an ordered tobermorite or xonotlite structure.

(3) A shift in the 2θ position (equivalent $d = 3.0–3.09$ Å) of the tobermorite (220) and/or the xonotlite (320) peak some time after the C–S–H gel has formed indicates ordering in the silicate and calcium octahedral layers. The increase in *d*-spacing is thought to reflect the inclusion of silicate tetrahedra into vacancies in the silicate chains as the sample progressively crystallises.

(4) Kinetic data calculated from the in situ synthesis reactions show that *k* increases with increasing aluminium contents of the starting material and increasing temperature. Activation energies for the formation of tobermorite and xonotlite range from 19 to 37 kJ/mol, depending on the stage of the crystallisation reaction they represent.

(5) In the context of waste disposal, it has been found that C–S–H gel buffers groundwater pH to approximately 11 (Atkinson et al., 1995), whereas crystalline tobermorite buffers to a lower pH of approximately 9. Therefore, the rate at which C–S–H gel transforms to tobermorite is critical when modelling the pH evolution of the groundwater surrounding a cement encapsulated waste site. This work shows clearly the influence of aluminium on the formation of both tobermorite and xonotlite. Therefore, the aluminium content of any cement used in waste disposal must be closely monitored as it may have a significant effect on the chemical evolution of the groundwater in and around a waste site.

Acknowledgements

This work was supported through NERC studentship GT4/96/202/E and through beam time awards from the NERC block grant to Daresbury

laboratory. Portions of this work were performed at GeoSoilEnviroCARS (GSECARS), Sector 13, Advanced Photon Source at Argonne National Laboratory. GSECARS is supported by the National Science Foundation — Earth Sciences, Department of Energy — Geosciences, W.M. Keck Foundation and the United States Department of Agriculture. Use of the Advanced Photon Source was supported by the U.S. Department of Energy, Basic Energy Sciences, Office of Energy Research, under contract no. W-31-109-Eng-38.

References

Atkinson, A., Harris, A.W., Hearne, J.A., 1995. Hydrothermal alteration and aging of synthetic calcium silicate hydrate gels. UK Nirex report NSS/R374.

Cheary, R.W., Coelho, A.A., 1992. A fundamental parameters approach of X-ray line-profile fitting. J Appl. Cryst. 25, 109–121.

Clark, S.M., 1996. A new energy-dispersive powder diffraction facility at the SRS. Nucl. Instrum. Methods Phys. Res., Sect. A 381, 161–168.

Clark, S.M., Nield, A., Rathbone, T., Flaherty, J., Tang, C.C., Evans, J.S.O., Francis, R.J., O'Hare, D., 1995. Development of large volume reaction cells for kinetics studies using energy-dispersive powder diffraction. Nucl. Instrum. Methods, Sect. B 97, 98–101.

Cong, X., Kirkpatrick, R.J., 1996. ^{17}O NMR investigation of the structure of calcium silicate hydrate. J. Am. Ceram. Soc. 79:, 1585–1592.

El-Hemaly, S.A.S., Mitsuda, T., Taylor, H.F.W., 1977. Synthesis of normal and anomalous tobermorite. Cem. Concr. Res. 7:, 429–432.

Evans, J.S.O., Francis, R.J., O'Hare, D., Price, Clark, S.M., Flaherty, J., Gordon, J., Nield, A., Tang, C.C., 1994. An apparatus for the study of the kinetics and mechanism of hydrothermal reactions by in-situ energy dispersive X-ray diffraction. Rev. Sci. Instrum. 66, 2442–2445.

Gabrovšek, R., Kurbus, B., Mueller, D., Weiker, W., 1993. Tobermorite formation in the system $CaO,C_3S–SiO_2–Al_2O_3–NaOH–H_2O$ under hydrothermal conditions. Cem. Concr. Res. 23, 321–328.

Gartner, E.M., Jennings, H.M., 1987. Thermodynamics of calcium silicate hydrate and their solutions. J. Am. Ceram. Soc. 70, 743–749.

Hamid, S.A., 1981. The crystal structure of 11 Å tobermorite $Ca_{2.25}[Si_3O_{7.5}(OH)_{1.5}]\cdot 1H_2O$. Zeit. Krist. 154, 189–198.

Hamilton, D.L., Henderson, C.M.B., 1968. The preparation of silicate compositions by a gelling method. Min. Mag. 36, 832–838.

Henmi, C., Kusachi, I., 1992. Clinotobermorite, $Ca_5Si_6(O,OH)_{18}\cdot 5H_2O$, a new mineral from Fuka, Okayama prefecture, Japan. Min. Mag. 56, 353–358.

Hoffman, C., Armbruster, T., 1997. Clinotobermorite, $Ca_5[Si_3O_8(OH)]_2\cdot 4H_2O–Ca_5[Si_6O_{17}]\cdot 5H_2O$, natural C–S–H (I) type cement mineral: determination of the substructure. Zeit. Krist. 212, 864–873.

Holland, T.J.B., Redfern, S.A.T., 1997. Unit cell refinement from powder diffraction data: the use of regression diagnostics. Min. Mag. 61, 65–77.

Jauberthie, R., Temimi, M., Laquerbe, M., 1996. hydrothermal transformation of tobermorite gel to 10 Å tobermorite. Cem. Concr. Res. 26, 1335–1339.

Klur, I., Pollet, B., Virlet, J., Nonat, A., 1998. C–S–H structure evolution with calcium content by multinuclear NMR. In: Colombet, P., Grimmer, A.R., Zanni, H. (Eds.), Nuclear Magnetic Resonance Spectroscopy of Cement-Based Materials. Springer, pp. 119–142.

Livingston, A., 1988. Reyerite, tobermorite, calcian analcime and bytownite from amygdales in a Skye basalt. Min. Mag. 52, 711–713.

Mamedov, K.S., Belov, N.V., 1955. Structure of xonotlite. Dokl. Akad Nauk SSSR 104, 615–618.

Mitsuda, T., Taylor, H.F.W., 1975. Influence of aluminium on the conversion of calcium silicate hydrate gels into 11 Å tobermorite at 90°C and 120°C. Cem. Concr. Res. 5, 203–210.

Mitsuda, T., Taylor, H.F.W., 1978. Normal and anomalous tobermorites. Min. Mag. 42, 229–235.

Taylor, H.F.W., 1990. Cement Chemistry. Academic Press, San Diego, CA.

Vieland, D., Li, J., Yuan, L., Zhengkui, X., 1996. Mesostructure of calcium silicate hydrate (C–S–H) gels in portland cement pastes: short-range ordering, nanocrystallinity, and local compositional order. J. Am. Ceram. Soc. 79, 1731–1744.